Performance Research of Planar 5R Parallel Mechanism with Variable Drive Configurations

Weitao Yuan[1,2], Zhaokun Zhang[1], Zhufeng Shao[1(✉)],
Liping Wang[1,2], and Li Du[2]

[1] Beijing Key Lab of Precision/Ultra-Precision Manufacturing Equipments
and Control, State Key Laboratory of Tribology, Tsinghua University,
Beijing 100084, China
shaozf@mail.tsinghua.edu.cn
[2] School of Mechatronics Engineering, University of Electronic Science
and Technology of China, Chengdu 611731, China

Abstract. All joints of the serial mechanism are active ones, while only some joints are active ones for the parallel mechanism. Thus, there is a variety of drive configurations with different active joint selections. Drive configuration will affect the performance of parallel mechanism and the effect deserves further study. A planar 5R parallel manipulator with the capability of adjusting drive configurations in real time is proposed in this paper. Based on the deduced Jacobian matrices, performances of the 5R parallel manipulator are analyzed, considering three symmetrical drive configurations. Typical kinematic performance indices, such as local conditioning index and kinematic manipulability, are adopted to give a complete illustration of the performance variation. Then, the optimal adjustment of driven configurations is proposed and studied, considering local conditioning index. Simulation results reveal that the performance of the 5R parallel manipulator improves obviously through the reasonable combination of different drive configurations in the workspace. The drive configuration adjustment proposed in this paper provides a novel potential way to enhance the comprehensive performance of the parallel mechanism.

Keywords: Planar 5R parallel mechanism · Drive configuration · Performance analysis · Kinematics

1 Introduction

Mechanisms can be divided into two categories: serial and parallel mechanisms. Serial mechanisms consist of drive joints with single degrees of freedom (DoFs). Each joint is an independent active joint. Joints are connected serially, and only a kinematic chain links the framework (base) and the terminal (end effector). The parallel mechanism is recognized as a significant complement to the serial mechanism because of the closed-loop kinematic chains in its structure [1, 2]. Parallel mechanisms are usually composed of a base and an end effector, which are connected with at least two identical

kinematic chains (branches) [3, 4]. Some joints are active ones, and passive joints that result in multiple available drive configurations exist. To reduce the mass and inertia of moving parts, the joints near the base are usually selected as active ones [5]. Studies on the performance analysis and optimal adjustment of different drive configurations are limited. However, drive configuration obviously affects the performance of parallel mechanism [6] and deserves further study.

Planar 5R parallel mechanism is preferred for the initial study of the parallel mechanism field because it possesses the advantages of simple structure, large workspace, good flexibility, absence of singularity in the reachable workspace [7], and easy control. For example, Zhang et al. [8] completed the theoretical and experimental research on the trajectory planning and kinematics simulation of the 5R mechanism. Ouyang et al. [9] performed dynamic analysis and studied the locomotive simulation problem of the 5R mechanism. Liu et al. [10–12] discussed the kinematics, singularity, and workspace of the 5R mechanism in detail. In general, the existing research on 5R mechanism covers position analysis, workspace, assembly pattern, singular research, dynamic analysis, and so on [13–16]. However, the research on the performance changes in different drive configurations is limited. By adding a facile transmission in the planar 5R mechanism, the real-time and flexible adjustment of drive configuration can be achieved without any change in the mass and inertia property of the mechanism. Variable drive configurations provide new possibilities for the performance improvement of the parallel mechanism and lead to new questions. How will the drive configuration affect the performance of parallel mechanism? How can the drive configuration be adjusted to achieve performance improvement? This study focuses on these questions.

In the process of analysis and optimal design, several indices, which are mainly kinematic indices, are inevitably adopted to illustrate the performance of the parallel manipulator [17]. The number of conditions in the kinematic Jacobian matrix is acknowledged as a comprehensive kinematic performance index and has been used by several researchers for optimum design. In addition, kinematic manipulability is also widely used as the supplement. The local conditioning index (LCI) was proposed by Gosselin and Angeles and has been used to evaluate the output isotropy of the parallel mechanism [18–20]. Yoshikawa defined the kinematic manipulability of a robot and analyzed the velocity transmission of the mechanism [21]. LCI and kinematic manipulator are adopted in this study to demonstrate the kinematic performance of the 5R parallel manipulator in different drive configurations.

The remainder of this paper is organized as follows. In the next section, the 5R parallel mechanism with variable drive configurations is introduced in detail, and the kinematic analysis is discussed. In the third section, the kinematic performances of the 5R parallel mechanism are illustrated and analyzed. LCI is taken as an example to verify the effect of performance improvement on the 5R parallel mechanism considering drive configuration adjustment. The conclusions drawn in this study are enumerated in the last section.

2 5R Mechanism with Variable Drive Configurations

2.1 Research Object

The virtual prototype of our object is shown in Fig. 1, which is actuated with two sets of AC servomotors and reducers. The basic structure is a planar 5R parallel mechanism, and the kinematic model is illustrated in Fig. 2. Two RRR branches exist (R represents revolute joint). In each branch, rod A_iB_i ($i = 1, 2$) and rod B_iP are connected directly by the revolute joint B_i, and rod A_iB_i is attached to the static framework with revolute joint A_i. The two branches connected by revolute joint P, which is also the end effector. To facilitate further analysis and description, the base coordinate system $O–XYZ$ is located at the center of A_1A_2 with the X-axis pointing toward point A_2, and the Y-axis is perpendicular to line A_1A_2. The geometric relations are defined as follows. $OA_1 = OA_2 = r_1$. The lengths of rods A_iB_i and B_iP are r_2 and r_3, respectively. $\boldsymbol{m}_i$ and $\boldsymbol{n}_i$ are the unit direction vectors of rods A_iB_i and B_iP, respectively. θ_i is the angle between vector $\boldsymbol{m}_i$ and the positive direction of the X-axis, while ψ_i is the angle between vectors $\boldsymbol{m}_i$ and $\boldsymbol{n}_i$. In this paper, vectors and matrices are in bold italics, while variables are in italics. The branch number is illustrated with the corresponding subscripts.
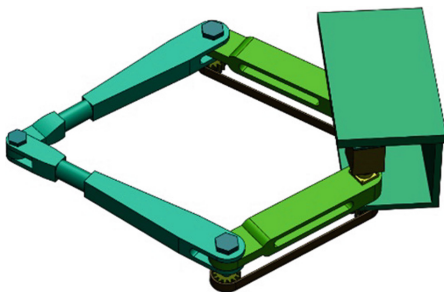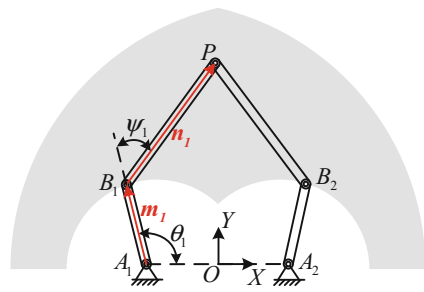

Fig. 1. Virtual prototype.

Fig. 2. Kinematic model.

Figure 3 illustrates the detailed structure of the branch. To adjust the drive configuration, the mechanism is equipped with the extra transmission system. The drive unit (servomotor and reducer) is attached to a cabin, which connects the static framework and the rod A_iB_i through electromagnetic clutches I and II, respectively. The power output shaft of the drive unit connects rod A_iB_i and pulley 1 with clutches III and IV separately. Pulley 2 is attached to rod B_iP as shown in the figure. The timing belt is adopted to transfer the rotation between two pulleys. The four clutches above are coaxial with joint A_i and pulley 2, while pulley 1 is coaxial with joint B_i. The clutches are controlled with the voltage signal, and can achieve real-time online control, which implements the power transmission path change and drives configuration variation.

When clutches I and III clasp (clutches II and IV release), the drive unit is equivalently fixed to the static framework, and the output shaft drives rod A_iB_i to rotate around joint A_i. Then, joint A_i becomes the active joint and the drive angle is θ_i, which
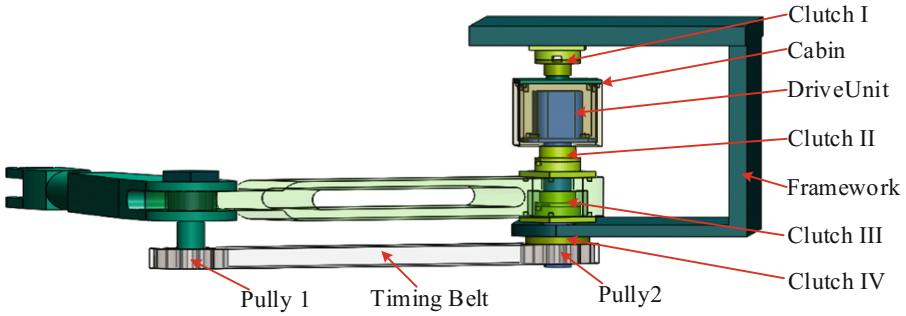
Fig. 3. Detailed drive structure of the branch.

is called branch drive mode 1. If clutches II and IV clasp (clutches I and III release), the drive unit is attached to rod A_iB_i and the output shaft connects rod B_iP through clutch IV and the belt system. In this situation, the drive unit is equivalently installed in joint B_i, the branch is driven by revolute joint B_i with drive angle ψ_i, which is called the branch drive mode 2. In addition, when clutches I and IV clasp (clutches II and III release), the drive unit is fixed to the static platform and the output shaft is connected to rod B_iP through clutch IV and the belt system. This is the branch drive mode 3, and the drive angle is $\theta_i - \psi_i$. To preserve the symmetrical characteristic of the 5R parallel mechanism, this study considers drive configurations I, II, and III when both branches successively employ branch drive modes 1, 2, and 3.

2.2 Kinematics Analysis

The kinematic analysis of this section focuses on deducing the Jacobian matrices under three drive configurations. According to the kinematic model in Fig. 2, the vector chain equation can be expressed as

$$p = \mu_i + r_2 m_i + r_3 n_i, \tag{1}$$

where μ_i is the position vector of point A_i.

The above equation can be simplified as

$$\tan \frac{\theta_i}{2} = \frac{-C_{i1} \pm \sqrt{C_{i1}^2 - (C_{i3}^2 - C_{i2}^2)}}{C_{i3} - C_{i2}}. \tag{2}$$

In addition, $C_{i1} = -2r_2(p - \mu_i) \cdot k_2$, $C_{i2} = 2(-1)^i r_2(p - \mu_i) \cdot k_1$, and $C_{i3} = (p - \mu_i)^2 + r_2^2 + r_3^2$ k_1 and k_2 are the unit direction vectors of the X-axis and the Y-axis, respectively. According to the assembly pattern of the 5R parallel mechanism, the positive and negative signs in Eq. (2) can be determined. Then, the inverse position solution of drive configuration I can be deduced as

$$\theta_i = 2\arctan\frac{-C_{i1} + \sqrt{C_{i1}^2 - (C_{i3}^2 - C_{i2}^2)}}{C_{i3} - C_{i2}}. \tag{3}$$

When the position vector $\boldsymbol{p}$ of the moving platform is provided, vector $\boldsymbol{n}_i$ can be deduced with Eqs. (1) and (3). At the same time, vector $\boldsymbol{n}_i$ can be expressed as

$$\boldsymbol{n}_i = \left[(-1)^{i+1}\cos(\theta_i - \psi_i) \quad \sin(\theta_i - \psi_i) \quad 0\right]^{\mathrm{T}}. \tag{4}$$

Input angle $\dot{\psi}_i$, which is also the inverse position solution of drive configuration II, can be derived as

$$\psi_i = \theta_i - \arcsin\boldsymbol{n}_i(2), \tag{5}$$

where $\boldsymbol{n}_i(2)$ is the second element of the $\boldsymbol{n}_i$ vector.

By sorting Eq. (5), $\theta_i - \psi_i$ can be obtained, which is the inverse position solution of drive configuration III. Taking the derivative of Eq. (1) with respect to time yields

$$\dot{\boldsymbol{p}} = r_2\dot{\theta}_{\mathrm{i}}(\boldsymbol{k}_3 \times \boldsymbol{m}_i) + r_3\left(\dot{\theta}_{\mathrm{i}} - \dot{\psi}_{\mathrm{i}}\right)(\boldsymbol{k}_3 \times \boldsymbol{n}_i), \tag{6}$$

where $\dot{\boldsymbol{p}}$ is the velocity vector of the moving platform. $\dot{\theta}_{\mathrm{i}}$, $\dot{\psi}_{\mathrm{i}}$ and $\dot{\theta}_{\mathrm{i}} - \dot{\psi}_{\mathrm{i}}$ denote the input angular velocities of drive configurations I, II, and III, respectively.

By taking the dot product of both sides of Eq. (6) with $\boldsymbol{n}_i$, $r_2\boldsymbol{m}_i + r_3\boldsymbol{n}_i$, $\boldsymbol{m}_i$, the following are respectively derived:

$$\boldsymbol{J}_1 = \left[\frac{\boldsymbol{n}_1^{\mathrm{T}}}{r_2(\boldsymbol{m}_1 \times \boldsymbol{n}_1) \cdot \boldsymbol{k}_3}; \frac{\boldsymbol{n}_2^{\mathrm{T}}}{r_2(\boldsymbol{m}_2 \times \boldsymbol{n}_2) \cdot \boldsymbol{k}_3}\right], \tag{7}$$

$$\boldsymbol{J}_2 = \left[\frac{-(r_2\boldsymbol{m}_1 + r_3\boldsymbol{n}_1)^{\mathrm{T}}}{r_3[\boldsymbol{n}_1 \times (r_2\boldsymbol{m}_1 + r_3\boldsymbol{n}_1)] \cdot \boldsymbol{k}_3}; \frac{-(r_2\boldsymbol{m}_2 + r_3\boldsymbol{n}_2)^{\mathrm{T}}}{r_3[\boldsymbol{n}_i \times (r_2\boldsymbol{m}_2 + r_3\boldsymbol{n}_2)] \cdot \boldsymbol{k}_3}\right], \tag{8}$$

$$\boldsymbol{J}_3 = \left[\frac{\boldsymbol{m}_1^{\mathrm{T}}}{r_3(\boldsymbol{n}_1 \times \boldsymbol{m}_1) \cdot \boldsymbol{k}_3}; \frac{\boldsymbol{m}_2^{\mathrm{T}}}{r_3(\boldsymbol{n}_2 \times \boldsymbol{m}_2) \cdot \boldsymbol{k}_3}\right], \tag{9}$$

Finally, we derive $\boldsymbol{J}_1$, $\boldsymbol{J}_2$, and $\boldsymbol{J}_3$, which are the Jacobian matrices of drive configurations I, II, and III, respectively. In the following section, the following dimension parameters are adopted: $r_1 = 0.55$ m, $r_2 = 0.8$ m, and $r_3 = 1.6$ m.

3 Kinematic Performance Analysis

3.1 LCI

As deduced in the previous section, the Jacobian matrix is the mapping between the input and output velocities. The LCI of the parallel mechanism is defined based on the

Jacobi matrix, which is adopted to describe the isotropy degree of the output velocity under a certain position. The number of conditions of the parallel manipulator can be described as

$$\kappa = \frac{\sigma_{\max}}{\sigma_{\min}}, \tag{10}$$

where $\sigma_{\max}$ and $\sigma_{\min}$ are the maximum and the minimum singular values of the Jacobian matrix, respectively. Thus, $1 \leq \kappa \leq \infty$. The LCI is defined as the reciprocal of the number of conditions of the Jacobian matrix. Therefore, when LCI = 1, the mechanism is isotropic. A large LCI value ensures a good control accuracy.

The LCI value distributions of the 5R mechanism with different drive configurations are illustrated in the reachable workspace, as shown in Fig. 4. From these figures, we know that:

(1) The drive configuration has an obvious impact on the LCI value distribution of the 5R parallel mechanism. In general, large values are in the center area for symmetrical drive configurations. This area is slightly low for configuration III.
(2) The maximum LCI values for drive configurations I and III are similar and nearly 1. However, the maximum LCI value for drive configuration II is significantly less. The average value of the LCI for drive configuration I is the largest among the average values of the configurations.
(3) Noticeable differences can be observed between the LCI distributions of drive configuration I and II. The 5R mechanism can improve the LCI value distribution and the isotropic performance by properly transforming the drive configurations in the reachable workspace.

3.2 Kinematic Manipulability

The product of the singular values of the Jacobian matrix defines the kinematic manipulability index. For the planar 5R parallel mechanism, the kinematic manipulability index can be written as

$$\Gamma = \sqrt{\det\left(\boldsymbol{JJ}^{\mathrm{T}}\right)} = \sqrt{\lambda_1 \lambda_2} = \sigma_1 \sigma_2, \tag{11}$$

where σ_1 and σ_2 are the singular values of the Jacobian matrix. λ_1 and λ_2 are the matrix eigenvalues. Kinematic manipulability is a local performance index, which indicates the velocity transmission characteristics of the mechanism from the active joints to the terminal. A large kinematic manipulability index value ensures a good high-speed feature and an improved velocity amplification ability for the mechanism under the position. Therefore, a high output velocity can be obtained with the same input velocity.
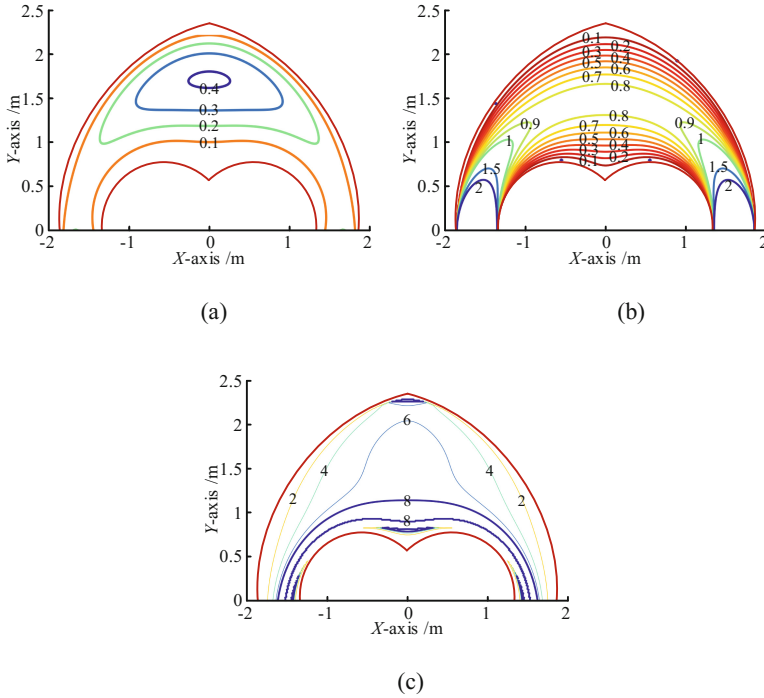
(a)

(b)

(c)
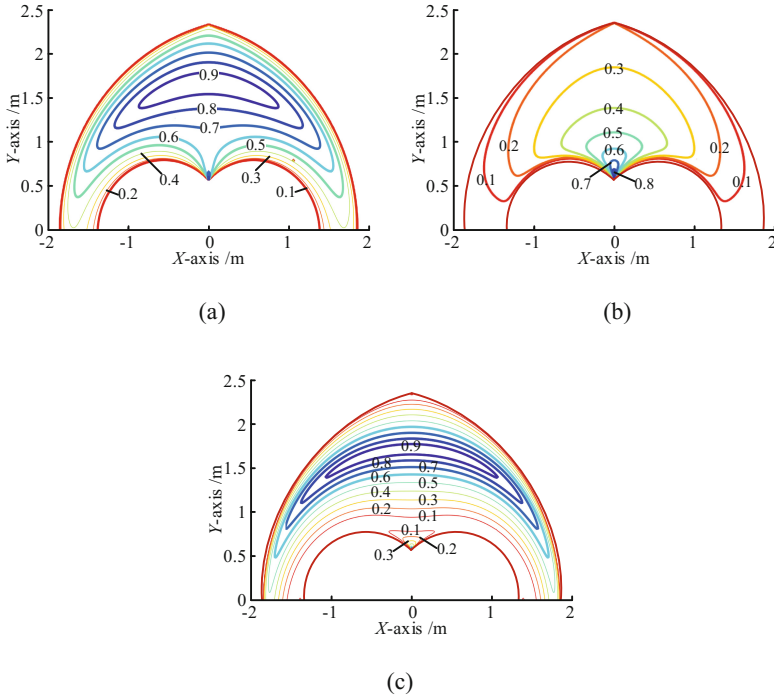
(a) Drive configuration I. (b) Drive configuration II. (c) Drive configuration III.

Fig. 4. The LCI value distribution.

The value distributions of the kinematic manipulability index for the planar 5R parallel mechanism are illustrated in Fig. 5. The comparative analysis of these curves indicates the following:

(1) Drive configuration significantly affects the value distribution of the kinematic manipulability index of the 5R parallel manipulator. Generally, the index values of drive configuration I are the smallest, while the index values of drive configuration III are the largest.

(2) In the value distribution of the index, the large values of drive configurations I and III are in the workspace center, while the large values of drive configuration II appear on both sides.

In all, the performance of the planar 5R parallel manipulator varies significantly with the drive configuration. In drive configuration I, the manipulator possesses the best isotropic property, while the best kinematic manipulability is acquired in drive configuration III. Drive configuration II is moderate in all. In addition, the performance of the parallel mechanism could be further improved by adjusting the drive configuration in the workspace appropriately.
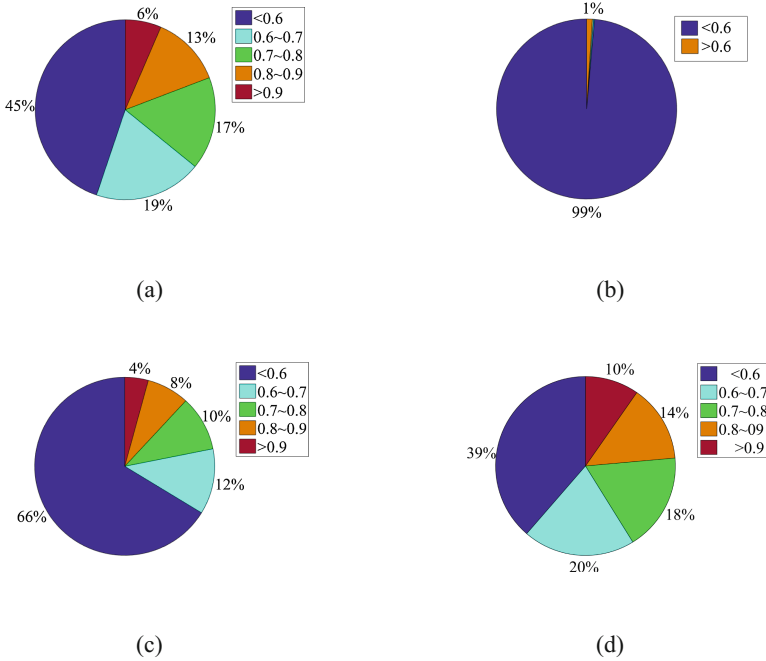
(a)

(b)

(c)

(a) Drive configuration I. (b) Drive configuration II. (c) Drive configuration III.

Fig. 5. The value distribution of the kinematic manipulability index.

4   Drive Configuration Adjustment

In this section, the kinematic performance improvement of the planar 5R mechanism is verified with the LCI, considering the drive configuration adjustment. The simulation parameters are given as $r_1 = 0.55$ m, $r_2 = 1.24$ m, and $r_3 = 2.34$ m. The LCI values in the reachable workspace are divided into five ranges. Figure 6 illustrates the area ratios of the LCI value ranges in four drive configurations, namely I, II, III, and the adjustment. Figure 7 shows the adopted drive configurations in the reachable workspace for the drive configuration adjustment. Drive configurations I and III are adopted in most of the reachable workspaces.

The comparative analysis in Fig. 6 shows that kinematic performance can be improved by adjusting the drive configuration. For example, the area ratios of the LCI value ≥ 0.8 for drive configurations I, II, and III are 19%, less than 1%, and 12%, respectively. The area ratios of the LCI values that are greater than or equal to 0.8 under the drive configuration adjustment achieves 24%, which is better than any single drive configuration. At the same time, the area ratio of the LCI value below 0.6 under the drive configuration adjustment is reduced to 39%. Drive configuration adjustment is a potential way to improve the performance of the parallel mechanism.

(a)

(b)

(c)

(d)

(a) Drive configuration I. (b) Drive configuration II. (c) Drive configuration III. (d) The adjustment of drive configuration
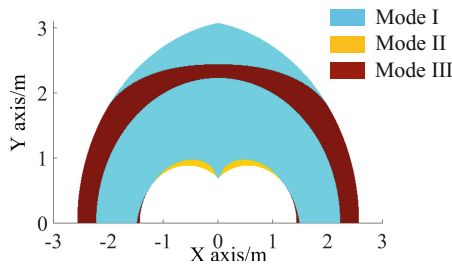
Fig. 6. Area ratios of the LCI value ranges.

Fig. 7. Configuration distribution of the drive configuration adjustment.

5   Conclusions

Kinematic performances of the planar 5R parallel mechanism under three symmetrical drive configurations are studied in the reachable workspace by adopting the LCI and kinematic manipulability index. The influence of drive configurations on the kinematic performance is illustrated and analyzed. Drive configuration adjustment is proposed as

a potential way to improve the performance of the parallel manipulator, and the simulation verification is given. Specific conclusions are as follows:

(1) By introducing the timing belt system and clutches, the planar symmetric 5R parallel mechanism is proposed, which can realize the real-time change of drive configurations. The Jacobian matrices for the 5R parallel mechanism are deduced under drive configurations I, II, and III.

(2) Drive configurations affect the mechanism performance significantly. Under drive configuration I, the 5R manipulator possesses the best isotropic property, while the best kinematic manipulability is acquired in drive configuration III. And, drive configuration II is moderate.

(3) Taking the LCI as an example, the effectiveness of the drive configuration adjustment to performance improvement is verified with numerical simulation. The drive configuration adjustment is a potential method to improve the performance of the parallel mechanism.

(4) More drive configurations will be analyzed in the future, and the optimal design of the 5R parallel mechanism will be studied considering the drive configuration adjustment.

References

1. Tsai, L.W.: Robot Analysis and Design: The Mechanics of Serial and Parallel Manipulators. Wiley, New York (1999)
2. Mo, J., Shao, Z.F., Guan, L.W., Xie, F.G., Tang, X.Q.: Dynamic performance analysis of the X4 high-speed pick-and-place parallel robot. Robot. Comput.-Integr. Manuf. **46**, 48–57 (2017)
3. Wu, J., Wang, J.S., You, Z.: An overview of dynamic parameter identification of robots. Robot. Comput. Integr. Manuf. **26**(5), 414–419 (2010)
4. Shao, Z.F., Tang, X.Q., Chen, X., Wang, L.P.: Research on the inertia matching of the Stewart parallel manipulator. Robot. Comput.-Integr. Manuf. **28**(6), 649–659 (2012)
5. Kuo, C.H., Dai, J.S.: Task-oriented structure synthesis of a class of parallel manipulators using motion constraint generator. Mech. Mach. Theory **70**(6), 394–406 (2013)
6. Chen, X.: Research on Transmission, Constraint and Output Performance Evaluation of Parallel Manipulator and Its Applications. Tsinghua University, Beijing (2015)
7. Liu, X.J., Wang, J.S.: Parallel Kinematics: Type, Kinematics and Optimal Design. Springer, Berlin (2014)
8. Zhang, L.J., Guo, Z.M., Li, Y.Q.: Trajectory planning, kinematic simulation and experiment research on planar 5R parallel manipulator. Mach. Des. Res. **29**(1), 10–13 (2013)
9. Quyang, P.R., Zhang, W.J., Wu, F.X.: Nonlinear PD control for trajectory tracking with consideration of the design for control methodology. In: Proceedings of the 2002 IEEE International Conference, vol. 4, pp. 4126–4131. Robotics and Automation, Washington DC, USA (2002)

10. Liu, X.J., Wang, J.S., Prischow, G.: Performance atlases and optimum design of planar 5R symmetrical parallel mechanisms. Mech. Mach. Theory **41**(2), 119–144 (2006)
11. Liu, X.J., Wang, J.S., Pritschow, G.: Kinematics singularity and workspace of planar 5R symmetrical parallel mechanisms. Mech. Mach. Theory **41**(2), 145–169 (2003)
12. Liu, X.J., Wang, J.S., Xie, F.G.: Analysis and kinematic optimization of planar 2-DoF 5R parallel mechanisms considering the force transmissibility. Optimization **41**(2), 453–461 (2001)
13. Alici, G.: An inverse position analysis of five-bar planar parallel manipulators. Robotica **20**(2), 195–201 (2002)
14. Cervantes-Sanchez, J.J., Hemandez-Rodriguez, J.C., Rendon-Sanchez, J.G.: On the workspace, assembly configurations and singularity curves of the RRRRR-type planar manipulator. Mech. Mach. Theory **35**(8), 1117–1139 (2000)
15. Gao, F., Zhang, X.Q., Zhao, Y.S.: A physical model of the solution space and the atlases of the reachable workspaces for 2-DoF parallel plane manipulator. Mech. Mach. Theory **31**(2), 173–184 (1996)
16. Park, F.C., Kim, J.W.: Singularity analysis of closed kinematic chains. J. Mech. Design **121**(1), 32–38 (1999)
17. Shao, Z.F., Tang, X.Q., Wang, L.P.: Atlas based kinematic optimum design of the Stewart parallel manipulator. Chin. J. Mech. Eng. **28**(1), 20–28 (2015)
18. Gosse, L.C., Angeles, J.: The optimum kinematic design of a spherical three-degree-of-freedom parallel manipulator. J. Mech. Design **111**(2), 202–207 (1989)
19. Khan, W.A., Angeles, J.: The kinetostatic optimization of robotic manipulators: the inverse and the direct problems. J. Mech. Design **128**(1), 168–178 (2006)
20. Shao, Z.F., Tang, X.Q., Wang, L.P.: Optimum design of 3-3 Stewart platform considering inertia property. Adv. Mech. Eng. **2013**, 249121 (2013)
21. Yoshikawa, T.: Manipulability of robotic mechanisms. Int. J. Robot. Res. **4**(2), 3–9 (1985)